Plastic classification via in-line hyperspectral camera analysis and unsupervised machine learning

Martin L. Henriksen [a], Celine B. Karlsen [a], Pernille Klarskov [b], Mogens Hinge [a],*

[a] *Plastic and Polymer Engineering, Department of Biological and Chemical Engineering, Aarhus University, Aabogade 40, DK-8200, Aarhus N, Denmark*
[b] *Terahertz Photonics, Department of Electrical and Computer Engineering, Aarhus University, Finlandsgade 22, DK-8200, Aarhus N, Denmark*

ARTICLE INFO

ABSTRACT

An increase in the quality of recycled plastic is paramount to address the global plastic challenge and applicability of recycled plastics. A potent approach is mechanical plastic sorting but sufficient analytical techniques are needed. This study applies unsupervised machine learning on short wave infrared hyperspectral data to build a model for classification of plastics. The model can successfully distinguish between twelve plastics (PE, PP, PET, PS, PVC, PVDF, POM, PEEK, ABS, PMMA, PC, and PA12) and the utility is further proven by recognizing three unknown samples (PS, PMMA, PC). The experimental setup is constructed similar to an in-line industrial setup, and the machine learning is optimized for minimal data processing. This ensures the industrial relevance and is a stepping-stone to solve the global plastic challenge.

1. Introduction

Plastics are commonly used materials in the modern society but only a minor amount of the consumer plastics are recycled into new products (plastic circular economy) [1–4]. The properties and price of plastics favor the use in disposable and single usage products, which regrettably accumulate as pollutants in our ecosystems due to poor waste handling [5–11]. The introduction of plastic circularity as a sustainable approach is challenged by consumer behavior, collection infrastructure, product design limitations, etc. [12,13].

In a typical recycling process, the plastic waste is downsized e.g. by chopping, washed, followed by flotation separation or mechanical sorting. The resulting plastic purities varies from 75 to 95 % by mass, but the industrial demands plastic purities of 95 %+ [14]. The main challenge is identification and analysis of the plastic waste stream at an industrial throughput. A common approach is a running conveyer belt with plastic waste and cameras mounted above to monitor the waste stream. The conveyer belt is normally monitored with a narrow band (or single band) near-infrared detector. It can be argued that expanding the number of spectral bands will enable unique plastic identification. Even so, only a few hyperspectral-imaging studies are reported in the literature that all conclude that the analysis could be transferred into industrial settings for plastic sorting.

It is demonstrated that polyolefins can be distinguished from other waste types e.g. wood and aluminum employing a hyperspectral analysis in the Vis/SWIR range from 400 to 1700 nm [15]. A further expansion of the number of plastic types was performed with inclusion of poly(vinyl chloride) (PVC), polystyrene (PS) in addition to the olefins polypropylene (PP) high- and low-density polyethylene (HDPE and LDPE, respectively). The plastics were analyzed with a hyperspectral camera in the range from 1000 to 2500 nm [16] and the implementation of a hierarchical model enabled identification of the individual plastic types. These plastic types and addition of poly(ethylene terephthalate) (PET) and poly(acrylonitrile-butadiene-styrene) (ABS) post-consumer waste plastics has also been analyzed via a hyperspectral camera in the range from 1000 to 2500 nm. A Fisher discrimination model was suggested after a heavy spectral data processing and a high ability (100 %) for plastic identification was observed [17]. In addition to plastic types (also including poly(lactate acid)), a study includes the challenge of identifying plastic types of black plastics [18]. A SWIR and MIR spectral range from 700 to 13,500 nm was applied with MIR measured as diffuse reflection (separate laboratory apparatus). It was found that plastics dyed black could only be distinguished with the help of MIR and that further equipment development is necessary for industrialization of MIR technology is needed.

In this study, it will be examined if detailed plastic-type recognition is possible via reflection imaging with a hyperspectral camera (HC) technology in the wavelength range from 955 to 1700 nm with a

---

* Corresponding author.
E-mail address: hinge@bce.au.dk (M. Hinge).

minimum of data processing – only applying a normalization and a Savitzky-Golay filter. Thus, thirteen commercially available plastic types have been imaged by an industrial HC on a moving conveyer belt. The spectral information is used to establish an unsupervised machine learning model (principal component analysis (PCA) and K-means clustering) to discriminate between the plastic types and to classify three unknown plastic samples. Fourier transformed infrared spectroscopy (FTIR), differential scanning calorimetry (DSC), and thermogravimetrical analysis (TGA) are solemnly used to document the polymer types and identify some additives in the plastics which can interfere with the HC model.

2. Materials and methods

The materials used and the sample preparation, is followed by the method for documentation based on FTIR, DSC, TGA, and HC. Finally, the use of HC to discriminate plastics via machine learning is described.

2.1. Materials

The thirteen commercially available plastics included in this study are listed in Table 1.

All materials were used as received or processed into disk-shaped plastic specimens.

2.2. Sample preparation

PP, ABS, PET, and PC samples were injection molded on a manually operated benchtop injection molder (Model A-100, Galomb inc., USA) into a custom-made mold (SI figure S1). The mold cavity was designed to make 3 mm thick disks of Ø 35 mm. The polymers' process temperatures (melt, mold) are PP (175 °C, r.t.), ABS (250 °C, r.t.), PET (260 °C, 40 °C), and PC (310 °C, 80 °C) and all samples were relaxed for a minimum of 24 h and stored in zip lock bags until testing. The remaining plastic types were supplied as disk specimens, except PS, which were obtained from a CD cover. To test the effect of surface roughness, five ABS disks were stabbed multiple times with a screwdriver giving deep (1−2 mm) surface indentations and another five ABS disks were filed with a wood rasp ripping up the surface.

2.3. Fourier transformed inferred spectroscopy

Fourier transformed infrared spectra (FT-IR) of the disks and unknown samples were collected in an attenuated total reflection (ATR) mode on an iS5 spectrophotometer (Thermo Fisher Scientific, USA) fitted with a ZnSe crystal (iD5, Thermo Fisher Scientific, USA). Background (n = 8) and sample measurement (n = 8) was measured with a resolution of 2 cm^{-1}. Wavelength dependent penetration depth and baseline were corrected with OMNIC (v. 9.2.98., Thermo Scientific, USA) built-in functions.

2.4. Differential scanning calorimetry

A sample of 5−10 mg (Sartorius, MSE125P-000-DU) was cut from the sample disks and sealed (Universal Crimper Press, PerkinElmer, USA) into aluminum pans (Pans and covers type: 02190041) prior to measurement. Samples were loaded in a DSC 8000 (PerkinElmer, USA) controlled by Pyris (v. 11.1.0.0488, PerkinElmer, USA), heated to T_{max}, then cooled and subsequently heated from −70 °C to T_{max} all scans at 20 °C min^{-1}. T_{max} being 250 °C for PVC, PVDF, POM N, and POM B; 300 °C for HDPE, PP, PS, ABS, PMMA, PET, and PA12; and 400 °C for PEEK and PC. The first derivative's apex (150 points average filtering) determined the inflection point glass transition temperature (T_g) and the second derivative's minimum (150 points average filtering) determined the melting temperature (T_m).

2.5. Thermogravimetric analysis

Samples of 5−10 mg (Sartorius, MSE125P-000-DU) are heated both in laboratory air and under nitrogen in a TG 209 F1 Libra (Netzsch, GE) from 35 °C to 800 °C, 10 °C min^{-1}. The first derivative's apex (50 points average filtering) determined inflection point degradation temperature (T_d).

2.6. Hyperspectral camera setup

The hyperspectral camera (HC) setup can be found in the supporting information and is operated in its own room to minimize the impact of changing temperature, humidity, and light.

The HC setup consisted of a 29 cm wide conveyer belt (Newtec, DK) for sample transportation and a line-scan hyperspectral camera equipped with a spectrograph (QiSpec, QT5022K-I320-SWIR, Qtechnology, DK). The geometrical resolution was 1.1 mm (across) by 0.9 mm (along the conveyer belt) and the spectral resolution was 8.3 nm from 955 to 1700 nm (Calibration information is given in SI). The samples were illuminated by two rows of four halogen spots (12 V, 20 W) illuminating the conveyer belt at a 45° angle. Prior to measurement a fully illuminate Teflon sample (white reference) and the darkroom signal (black reference) were measured.

2.7. Hyperspectral polymer analysis

In a typical experiment, the samples were loaded on the conveyer belt, all other lights than the halogen lamps are turned off, and the samples passed by the scan line at a speed of 3.75 m min^{-1}, and the raw data was transferred to a laptop computer. The spectral signal for each disk was summarized over 200 pixels. The signal was then intensity corrected (black and white reference), vignette adjusted, and transformed into an absorbance spectrum ($A = \log(I_0/I)$), which is reported.

2.8. Hyperspectral identification via machine learning

The spectra are recorded as in 2.6.1., with the only two differences of 1) being kept as reflectance and 2) cropped to 972–1675 nm. The spectra are then normalized to span from zero to one, and the signal are Savitzky-Golay filtered [19] (width: 9, polynomial degree: 1, differentiation order: 1) to enhance the signal-to-noise ratio. Finally, the obtained principal components (PCA, Python, four principal components) are visualized in a score plot. The loading matrix was extracted and applied to post-process the unknown sample spectra (U1, U2, and U3 in Table 1). The thirteen cluster centroids (one centroid per plastic type)

Table 1
Plastic identification, plastic type, trade name, supplier for the materials included in this study.

ID	Plastic type	Name	Supplier
HDPE	Polyethylene	PE 100	SIMONA
PP	Polypropylene	240-CA12	INEOS
PS	Polystyrene	CD cover	–
PVC	Poly(vinyl chloride)	PVC-U	GEHR
PVDF	Poly(vinylidene difluoride)	PVDF	GEHR
POM N	Polyoxymethylene	Ertacetal C	Mitsubishi
POM B	Polyoxymethylene	Ertacetal C	Mitsubishi
PEEK	Polyetheretherketone	Ketron PEEK 1000	Mitsubishi
ABS	Poly(acrylonitrile-butadiene-styrene)	Terluran GP35	INEOS
PMMA	Poly(methyl methacrylate)	Setacryl 1000	Madreperla
PC	Polycarbonate	Makrolon 2652	Covestro
PET	Poly(ethylene therphalate)	CB-602	UltraPurge
PA12	Polyamide 12	PA 12-TR	GEHR
U1	Unknown	Weighing boat (White)	VWR
U2	Unknown	Plexiglas	Rias
U3	Unknown	Safety glasses	VWR

were estimated via K-means (Python, 13 clusters, K-means intelligent seed values, and random state: 42).

3. Results

FT-IR spectra from all materials are stacked in Fig. 1.

The spectra in Fig. 1 (detailed spectra is given in SI) are assigned as follows. **HDPE:** The bands at 2915, 2848, 1465, and 719 cm^{-1} are ascribed to stretch (ν) and bending (δ) of CH$_2$. **PP:** Additional bands compared to HDPE are found at 2916, 2866, and 1375 cm^{-1} and is ascribed to $\nu + \delta$CH$_3$ side chain and the $\nu + \delta$CH backbone [20]. **PS:** Similar backbone bands to HDPE and additional bands at 3082, 3058, 3024, 1600, and 1492 cm^{-1} are ascribed to the aromatic $\nu + \delta$CH$_{ar}$ and aromatic ring bend. The five overtones from 1660 to 1940 cm^{-1} and the band at 756, and 696 cm^{-1} are assigned to the *mono*-substituted aromatic ring. **PVC:** Similar backbone bands to HDPE (shifted with $\approx$ -30 cm^{-1}) and additional bands at 1331, 1097, 966, and 610 cm^{-1} and the thermostabilizing additive is found at 1732, 1258 and 1186 cm^{-1} and with some overlap at $\nu + \delta$CH$_2$, and $\nu + \delta$CH bands in PVC [20–23]. **PVDF:** Weaker bands near 2950 cm^{-1} and a stronger band at 1396 cm^{-1} for δCH$_2$ compared to HDPE, further bands at 1277, 1178, 1068, 874, and 840 cm^{-1} are ascribed to $\nu + \delta$C-F [20]. **POM:** Similar backbone bands to HDPE and additional ether bands at 1235, 1091, 924, 895, and 631 cm^{-1} [20,24]. **PEEK:** Bands found at 3060, 1595, 1488, and 765 cm^{-1} are ascribed to *para*-disubstituted benzene rings, the band at 1652 cm^{-1} is ascribed to νC=O, and the six bands from 1300 to 1000 cm^{-1} are ascribed to νC-O. [20,25]. **ABS:** Similar bands to PS and additional at 2250 cm^{-1} from the acrylonitrile, and bands between 1680−1620 cm^{-1} (νC=C) and at 912 (1,2-PB) and 967 cm^{-1} (1,4-PB) from polybutadiene [26]. **PMMA:** Similar bands to PP (slightly shifted and without CH) and additional bands at 1721 cm^{-1} from νC=O and 1237, 1195, and 1145 cm^{-1} from the νC—O in the ester group. **PC:** νC=O is found at 1771 cm^{-1}, νC-O found from 1000 to 1300 cm^{-1}, and the *para*-disubstituted benzene is similar to that of PEEK except for the weak band at 1600 cm^{-1}. **PET:** Similar backbone bands to HDPE and additional bands at 1712 cm^{-1} ascribed to νC=O, the bands at 1240 and 1095 cm^{-1} ascribed to νC—O, and the *para*-disubstituted benzene similar to PEEK, except the band at 766 cm^{-1} is shifted to 723 cm^{-1}. **PA12:** Similar backbone bands to HDPE and additional bands at 3230 cm^{-1} νNH and δNH at 1537 cm^{-1} (with overtone at 3077 cm^{-1}) and a band at 1639 cm^{-1} ascribed to νC=O [20].

Glass transition temperature (T$_g$), melting temperature (T$_m$), and decomposition temperature (T$_d$) found via DSC and TGA are listed in

Table 2

Glass transition temperature (T$_g$), melting temperature (T$_m$), and decomposition temperature (T$_d$) for the materials analyzed by differential scanning calorimetry (DSC) and thermogravimetrical analysis (TGA). TGA data is given as the T$_d$ (mass loss%).

	T$_g$ [°C]$^{\alpha}$	T$_m$ [°C]$^{\alpha}$	T$_d$ [°C]$^{\beta}$	T$_d$ [°C]$^{\gamma}$
HDPE	–	138	427 (100)	473 (100)
PP	–	149	328 (100)	458 (100)
PS	101	–	367 (100)	415 (98)
PVC	82	–	284 (59) 433 (36)	292 (59) 468 (23)
PVDF	–	172	404 (57) 558 (41)	452 (68)
POM N	–	169	285 (94)	355 (99)
POM B	–	170	313 (100)	357 (100)
PEEK	–	341	580 (31) 661 (94)	592 (45)
ABS	110	–	411 (92) 552 (8)	428 (93)
PMMA	129	–	317 (100)	374 (99)
PC	149	–	506 (73) 618 (100)	513 (80)
PET	86	250	428 (85) 574 (100)	438 (84)
PA12	159	–	420 (93) 535 (100)	437 (98)

$^{\alpha}$ DSC at 20 °C min^{-1}.
$^{\beta}$ TGA at 20 °C min^{-1} in air.
$^{\gamma}$ TGA at 20 °C min^{-1} in N$_2$.

Table 2 (details are given in SI).

The thermal properties in Table 2 show that there is low to no content of additives like softeners, fillers, etc. present in the applied polymers. [27]

The materials are analyzed with the industrial HC setup, and Fig. 2 shows the HC image of four disks at 1204 nm and the spectra of POM N.

Fig. 2 illustrates an example of a HC image of four sample disks and the area over which the spectral averaging is performed (left). The need for averaging to enhance the signal-to-noise ratio is seen as a reduction of noise as spectra are summarized. When averaging over 216 mm^2 (200 pixel) the spectral information becomes evident. In addition, the average and standard deviation of 1032 spectra measured on POM N is given in the supporting information.

Ten ABS disks have been imaged sequentially and their spectra are shown in Fig. 3.

From Fig. 3 it is found that there is a high reproducibility of spectral data for the ten ABS samples. The spikes on Disk 3 at 1590 nm, Disk 2 at 1680 nm, and Disk 7 at 1680 nm are ascribed to a channel blackout in one of the camera pixels applied in the summation.

The HC spectra obtained from the disks with modified surfaces are given in Fig. 4.

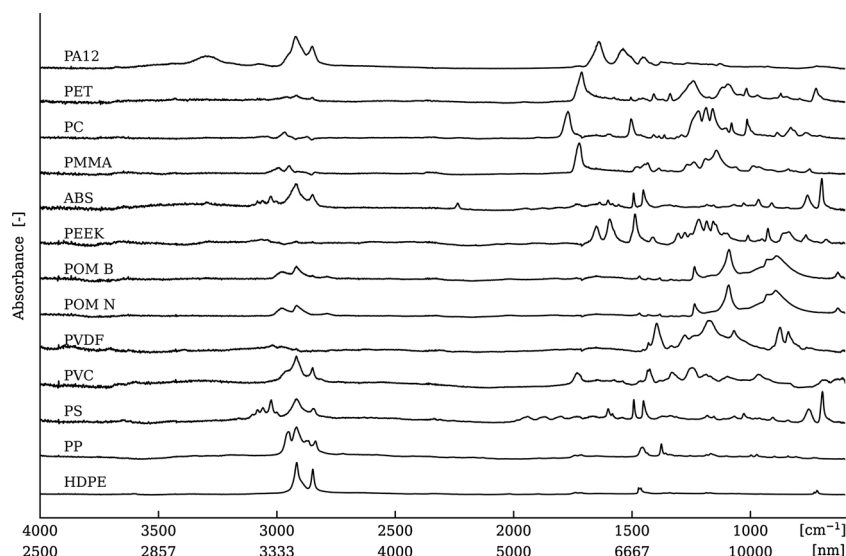The different surface textures of the ABS disks results in a minor shift

Fig. 1. FT-IR spectra for the materials tested. The spectra are shifted for visual clarity.
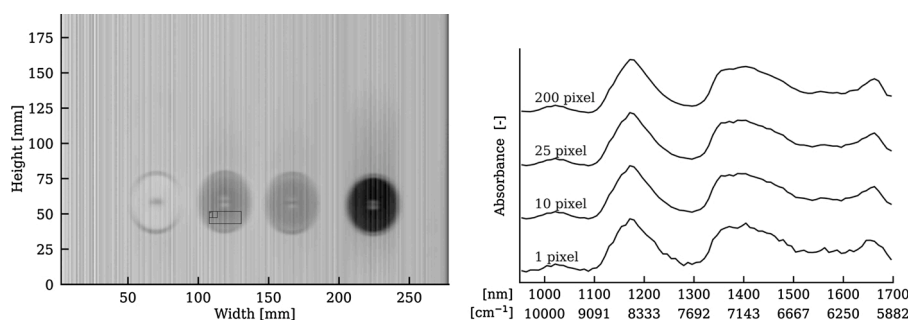
Fig. 2. Left, four disks (left to right: PEEK, POM N, POM N, and POM B) presented at 1204 nm and POM N (marked with the area of averaging). Right, hyperspectral spectrum of POM N from scans averaged over 1, 10, 25, and 200 pixels, respectively.
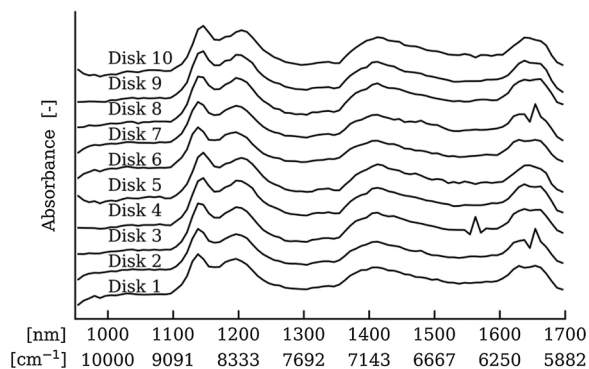

Fig. 3. Shows the spectra measured on ten different ABS specimens, each spectrum is an average of 200 pixels.
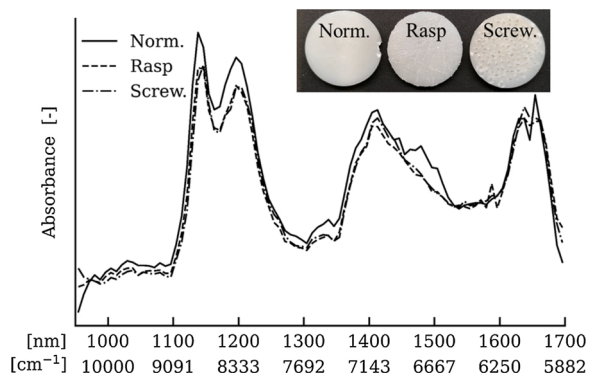

Fig. 4. Average spectra measured 10 ABS samples (Norm.), 5 ABS samples surface treated with a wood rasp (Rasp), and 5 ABS samples surface treated with screwdriver indentations (Screw.).

in the overall spectral intensities (Fig. 4), however, the spectral information is identical. The intensity ratio between the bands at 1150 nm (aromatic) and 1230 nm (aliphatic) is 1.008 ± 0.001, 1.006 ± 0.0004, and 1.007 ± 0.002 for untreated, rasped, and indented ABS disks, respectively.

All 13 materials in Table 1 were analyzed via industrial HC imaging and the spectra are given in Fig. 5.

The spectra in Fig. 5 (detailed spectra is given in SI) are assigned as follows. **HDPE:** The bands at 1180 and 1220 nm are ascribed to $3\nu CH_2$ and bands at 1050, 1400, 1420, and 1550 nm is ascribed to combination (com.) bands from $\nu + \delta CH_2$, the band at 1670 nm is ascribed to $2\nu CH_2$ overtones [28]. **PP:** In addition to HDPE, bands for $3\nu CH_3$ at 1190, com. at 1490 nm and $3\nu CH_3$ at 1660 nm [28] (CH has weak bands at 1160 and 1490 nm). **PS:** Similar bands to HDPE and bands at 1160 ($3\nu CH_{ar}$) and 1660 ($2\nu CH_{ar}$) nm from CH in the benzene ring and com at 1520 nm

[28]. **PVC:** Slightly downshifted bands for CH and CH_2 compared to HDPE [28]. **PVDF:** Even larger downshift ($3\nu CH$) than PVC in addition to a larger intensity of the band at 1680 nm ($2\nu CH_2$) [28]. **POM:** Similar bands to HDPE and additional bands at 1230 ($3\nu H_2$-C-O) and 1375 nm (com) and an enhanced intensity at 1690 nm ($2\nu CH_2$) [28]. **ABS:** Has a higher intensity at 1650 nm compared to PS and additional band at 1680 nm from cis butadiene [28]. **PMMA:** Similar bands to PP and additional bands at 1150 ($5\nu C{=}O$, weak), 1190 ($3\nu H_3 C{-}O$), and 1450 nm ($4\nu C{=}O$) [28]. **PC:** Bands are found at 1150, 1330, 1680 nm for $3\nu CH_{ar}$, $3\nu CH_3$, and $2\nu CH_{ar}+2\nu CH_3$, respectively and combination bands from $1390-1550$ nm including the band from $4\nu C{=}O$ in the esters [28]. **PET:** Similar bands to HDPE and additional bands at 1150 and 1660 nm from the aromatics [28]. **PA12:** Similar bands to HDPE with the addition of bands ascribed to the amide at 1025 ($3\nu NH$), 1430 ($2\nu_s NH$), 1470 ($2\nu_a NH$), 1540, 1570, 1595, and 1620 nm ascribed to the Amid II band overlapping with the CH_2 com. [28].

A score plot of the PCA on the obtained spectra after Savitzky-Golay filtering is given in Fig. 6.

The score plot in Fig. 6 shows that the plastic types cluster with good separation. However, it is evident that PS, PC, ABS, and PET cluster close together in the center of the score plot due the presence of both aromatics and aliphatic groups. Further, Fig. 6 shows that the unknown samples are assigned to their respective clusters; U1 is assigned to PS, U2 assigned to PMMA, and U3 is assigned to PC. Although, U2 is close to PVDF in Fig. 6 the model prediction is based on all four principal components. Thus, U2 is correctly predicted to PMMA.

4. Discussion

This study is based on industrial available materials that might contain a broad range of additives, thus material verification was necessary. It is clear from the TGA results that the materials included (Table 1) were all fully decomposed (Table 2 and SI). It is further seen that oxygen in many cases (as expected) resulted in more thermal stable decomposition products giving rise to multiple mass loss steps. Independent of decomposition atmosphere, the 100 % mass loss documents that the materials contained no (or insignificant) amount of inorganic additives. The DSC results (see Table 2) showed insignificant shifts in T_g and T_m compared to literature values [27]. This indicates that there are low or insignificant concentrations of organic additives (e.g. softeners) in the included materials. However, for PVC there is (as expected) clear FTIR signals (see Fig. 1 and SI for more spectral detail) from the thermal stabilizers, which may have shifted the melting point to a lower value. In combination FTIR, DSC, and TGA results show that the included materials have no (or low) contaminant concentrations and they can be applied as commercially available plastics representing the different polymeric types.

The image pixel size is 1.1 mm by 0.9 mm but due to noise, it is not possible to obtain clear spectra from only one pixel. Enhancing the spectral signal-to-noise ratio by spectra summarization over a number of pixels to obtain clear spectral information is the limiting factor for
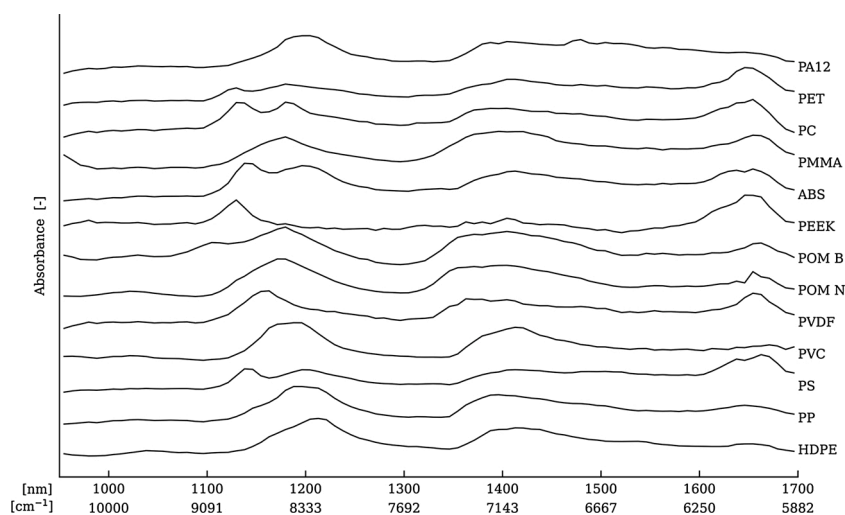
Fig. 5. Hyperspectral spectra for all materials, averaged over 200 pixel and shifted for visual clarity.
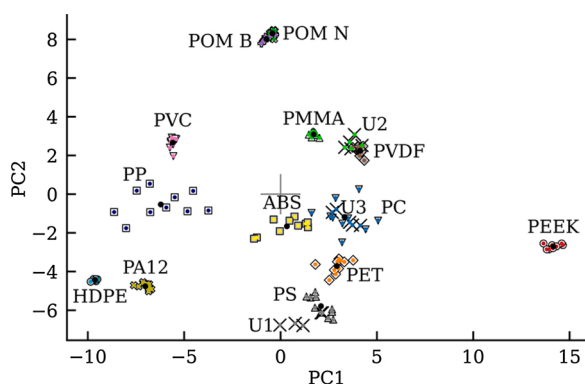

Fig. 6. Score plot of the first and second principal component (PC1 and PC2, respectively) from the principal component analysis made on the Savitzky-Golay filtered HC spectra. Calculated cluster centers (black circle), the unknown samples (X), symbols are the known material type, and a color is assigned to the predicted material type.

minimum geometrical dimensions of the plastic materials. Thus, elements larger than 27 mm² (25 pixel) are necessary for achieving a sufficient signal-to-noise ratio for the discrimination model. It is seen that averaging does not eliminate the dead pixel error (even after summarization of 200 spectra, Fig. 3), the reason is that the dead pixel is include in every line scanned across the conveyer belt. It is important to include these artifacts in the data handling, as they are present in all SWIR sensors.

The spectral quality as a function of surface roughness and texture were investigated and showed that despite an overall intensity reduction, presumably due to light scattering, the spectral information remained intact (Fig. 4). More important it was observed that even severer surface changes only gave a minor intensity reduction. It is clear that further investigation with a wider range of geometries, surface treatments, etc. are called for prior to industrialization of the technique. Most of the examined plastics are in a pure form, but POM was included as both neutral and blue POM (Table 1 and Fig. 5). The PCA (Fig. 6) shows that POM made a dense cluster independent of color. TGA results show that POM is colored with an organic dye (no residue after burning or pyrolysis) and organic dyes normally contain conjugated aromatic systems. Thus, it is a plausible expectation that the organic dye will absorb around 1160 ($3\nu CH_{ar}$) and 1660 ($2\nu CH_{ar}$) nm where POM has no absorbance (Fig. 5). However, the results indicate that the effect of plastic pigmentation on the spectral information is not interfering with

the first two principal components in the PCA as both POM neutral and blue are on top of each other in the score plot.

As described, color, surface texture, and shape all influence the overall intensity of the obtained spectral data. In the current system, it is possible to reduce the speed of the conveyer belt and thereby enhancing the ordinate (along the conveyer belt) resolution (Fig. 2 right) i.e. giving more pixel rows for spectral noise reduction. This approach is challenged by a reduction in material throughput and is therefore of low industrial relevance. The size and speeds are to be determined and optimized in the individual applications. Further, the reduction in speed will not eliminate the dead pixel noise. Small variations in the obtained spectra are found at lowest and highest wavelengths due to the sensitivity if the InGaAs sensor, thus the spectra are cropped from 955−1700 nm to 972−1675 nm prior to PCA. Further, the signal-to-noise ratio is maximized by applying a Savitzky-Golay filtering of the spectra. This means that spectral summation, normalization, and Savitzky-Golay filtering is the only data processing necessary for obtaining a full material classification via unsupervised machine learning (Fig. 6). This is key in obtaining an industrial relevant sorting algorithm i.e. reduce data processing time to a minimum while maintaining maximum material classification. It can be argued (Fig. 5) that spectral information between the overtones and combination bands could be discarded as they do not carry any material information and thus do not participate in the decision-making algorithm. This will result in a reduction of the demanded data processing, increase the sampling rate, and thereby resulting in a better spectral quality or higher material throughput.

The resulting score-plots from the PCA showed that normalization and Savitzky-Golay filtering significantly improved the grouping of polymer types compared to the analysis of raw spectra. However, the close grouping of PC, PS, and ABS increase the uncertainties in distinguishing between these plastic types. On the other hand, the K-means algorithm does determine all the centers correctly if the number of clusters are defined to the thirteen number of materials. If there is no maximum number of clusters allowed then the K-means algorithm finds 14 cluster by dividing the PP cluster into two. This indicates that the three aromatic containing plastics are statistically separated into separate groups. It is unclear why the PP data have a less dense cluster in the score plot (Fig. 6), but this low density is acceptable as the PP cluster is isolated in the upper part of the third quadrant of the score plot.

The unknown samples (U1, U2, and U3) were selected by random in the laboratory and imaged after the machine learning model was made, approximately a month after the reference plastics were measured. Based on the PCA of the unknown samples it is clear that U1 is PS, U2 is PMMA, and U3 is PC. From the IR spectra (given in SI) verify that U1 is PS, U2 is PMMA, and that U3 is PC. The random material selection with

no sample preparation, the time and day of imaging, and the fact that the samples were unknown until the day of imaging, demonstrates the predictive quality of the model. Further, the industrial potential is clearly demonstrated as all samples are imaged on a running conveyer belt using an industrial spectrograph, the data processing is kept at a minimum, and the machine learning shows its strong predictive power to discriminate between plastic types.

5. Conclusion

Hyperspectral imaging with wavelengths from 955 to 1700 nm on thirteen different plastics analyzed by PCA has shown that the spectral range is sufficient to differentiate plastics. Camera artifacts, sample area, and surface roughness/texture have an impact on the recorded spectra, and a Savitzky-Golay filter was successfully applied to minimize the impact from these variances and to emphasize the differences in overtones arising from the different polymer types. Unsupervised machine learning has proven to cluster the plastic types and the resulting loading matrix correctly classified unknown plastic samples. As all hyperspectral, imaging is performed with an industrially available spectrograph and with a minimum of data processing, it can be concluded that this evolving technology is the right tool to tackle the recycled plastic purity and thereby the global plastic challenge.

Author statement

The authors herby confirm that this work is original and that all creative ideas, designs, experimental work, data handling, etc. is performed by the authors and that there are no financial or ethical conflicts of interest.

We confirm that this article has not been published previously or is not under consideration elsewhere and has the full consent of all authors. If accepted it will not be published elsewhere in the same form, in English or in any other language, without the written consent.

Finally, the authors have revised the manuscript according to the reviewer's comments. A details response is given in the uploaded review report.

Data availability

The authors are unable or have chosen not to specify which data has been used.

CRediT authorship contribution statement

Martin L. Henriksen: Conceptualization, Methodology, Investigation, Resources, Formal analysis, Software, Writing - original draft, Writing - review & editing, Visualization. **Celine B. Karlsen:** Investigation, Formal analysis, Software, Visualization. **Pernille Klarskov:** Conceptualization, Project administration, Funding acquisition. **Mogens Hinge:** Conceptualization, Methodology, Investigation, Resources, Project administration, Funding acquisition, Writing - original draft, Writing - review & editing, Visualization.

Declaration of Competing Interest

The authors report no declarations of interest.

Acknowledgements

Appendix A. Supplementary data

Supplementary material related to this article can be found, in the online version, at doi:https://doi.org/10.1016/j.vibspec.2021.103329.

References

[1] I. Auken, Danmark uden affald, Miljø- Og Fødevareministeriet. 14 (2013) 1–40.

[2] F. Besenbacher, Advisory Board for cirkulær økonomi - Anbefalinger til regeringen, Miljø- Og Fødevareministeriet. (2017) 1–64.

[3] G. Leone, J.M.T. Borràs, E. de V. Martín, The New Plastics Economy: Rethinking the Future of Plastics & Catalysing Action, 2017.

[4] S.A. Veltzé, C. Fischer, S. Hirsbak, Miljøets fodspor nr. 5 - Affald, Miljøstyrelsen, 2019, pp. 1–36.

[5] D.K.A. Barnes, A. Walters, L. Gonçalves, Macroplastics at sea around Antarctica, Mar. Environ. Res. 70 (2010) 250–252, https://doi.org/10.1016/j.marenvres.2010.05.006.

[6] A.S. Colferai, R.P. Silva-Filho, A.M. Martins, L. Bugoni, Distribution pattern of anthropogenic marine debris along the gastrointestinal tract of green turtles (Chelonia mydas) as implications for rehabilitation, Mar. Pollut. Bull. 119 (2017) 231–237, https://doi.org/10.1016/j.marpolbul.2017.03.053.

[7] P.L. Corcoran, M.C. Biesinger, M. Grifi, Plastics and beaches: a degrading relationship, Mar. Pollut. Bull. 58 (2009) 80–84, https://doi.org/10.1016/j.marpolbul.2008.08.022.

[8] E. Martinez, K. Maamaatuaiahutapu, V. Taillandier, Floating marine debris surface drift: Convergence and accumulation toward the South Pacific subtropical gyre, Mar. Pollut. Bull. 58 (2009) 1347–1355, https://doi.org/10.1016/j.marpolbul.2009.04.022.

[9] P.G. Ryan, C.J. Moore, J.A. van Franeker, C.L. Moloney, Monitoring the abundance of plastic debris in the marine environment, Philos. Trans. R. Soc. B Biol. Sci. 364 (2009) 1999–2012, https://doi.org/10.1098/rstb.2008.0207.

[10] SUSCHEM, Sustainable Plastics Strategy, 2020.

[11] R.C. Thompson, Y. Olson, R.P. Mitchell, A. Davis, S.J. Rowland, A.W.G. John, D. McGonigle, A.E. Russell, Lost at sea: where is all the plastic? Science (80-.) 304 (2004) 838, https://doi.org/10.1126/science.1094559.

[12] European Commission, A european strategy for plastics in a circular economy, Eur. Comm. (2018).

[13] McKinsey & Company, The New Plastics Economy, 2019, pp. 1–69.

[14] M. Tsakona, I. Rucevska, Baseline report on plastic waste, Basel Conv. (2020) 1–61.

[15] S. Serranti, A. Gargiulo, G. Bonifazi, Characterization of post-consumer polyolefin wastes by hyperspectral imaging for quality control in recycling processes, Waste Manag. 31 (2011) 2217–2227, https://doi.org/10.1016/j.wasman.2011.06.007.

[16] G. Bonifazi, G. Capobianco, S. Serranti, A hierarchical classification approach for recognition of low-density (LDPE) and high-density polyethylene (HDPE) in mixed plastic waste based on short-wave infrared (SWIR) hyperspectral imaging, Spectrochim. Acta - Part A Mol. Biomol. Spectrosc. 198 (2018) 115–122, https://doi.org/10.1016/j.saa.2018.03.006.

[17] Y. Zheng, J. Bai, J. Xu, X. Li, Y. Zhang, A discrimination model in waste plastics sorting using NIR hyperspectral imaging system, Waste Manag. 72 (2018) 87–98, https://doi.org/10.1016/j.wasman.2017.10.015.

[18] O. Rozenstein, E. Puckrin, J. Adamowski, Development of a new approach based on midwave infrared spectroscopy for post-consumer black plastic waste sorting in the recycling industry, Waste Manag. 68 (2017) 38–44, https://doi.org/10.1016/j.wasman.2017.07.023.

[19] A. Savitzky, M.J.E. Golay, Smoothing and differentiation of data by simplified least squares procedures, Anal. Chem. 36 (1964) 1627–1639, https://doi.org/10.1021/ac60214a047.

[20] G. Socrates, Infrared and Raman Characteristic Group Frequencies: Tables and Charts, 3rd edition, John Wiley & Sons, 2004.

[21] B. Ruxanda, C.A. Teacă, I. Spiridon, Preparation and characterization of composites comprising modified hardwood and wood polymers/poly (vinyl chloride), BioResources 4 (2009) 1285–1304, https://doi.org/10.15376/biores.4.4.1285-1304.

[22] M.R. Jung, F.D. Horgen, S.V. Orski, V. Rodriguez C, K.L. Beers, G.H. Balazs, T. T. Jones, T.M. Work, K.C. Brignac, S.J. Royer, K.D. Hyrenbach, B.A. Jensen, J. M. Lynch, Validation of ATR FT-IR to identify polymers of plastic marine debris, including those ingested by marine organisms, Mar. Pollut. Bull. 127 (2018) 704–716, https://doi.org/10.1016/j.marpolbul.2017.12.061.

[23] R.R. Stromberg, S. Straus, B.G. Achhammer, Infrared spectra of thermally degraded poly(Vinyl chloride), J. Res. Natl. Bur. Stand. 60 (1958) (1934) 147–152.

[24] Y. Li, T. Zhou, Z. Chen, J. Hui, L. Li, A. Zhang, Non-isothermal crystallization process of polyoxymethylene studied by two-dimensional correlation infrared spectroscopy, Polymer (Guildf). 52 (2011) 2059–2069, https://doi.org/10.1016/j.polymer.2011.03.007.

[25] A.M. Diez-Pascual, G. Martínez, M.A. Gómez, Synthesis and characterization of poly(ether ether ketone) derivatives obtained by carbonyl reduction, Macromolecules 42 (2009) 6885–6892, https://doi.org/10.1021/ma901208e.

[26] J.G. Bokria, S. Schlick, Spatial effects in the photodegradation of poly(acrylonitrile-butadiene-styrene): a study by ATR-FTIR, Polymer (Guildf) 43 (2002) 3239–3246, https://doi.org/10.1016/S0032-3861(02)00152-0.

[27] J. Brandrup, E.H. Immergut, E.A. Grulke, Polymer Handbook, 4th edition, John Wiley & Sons, 2003.

[28] J. Workman Jr., L. Weyer, Practical Guide and Spectral Atlas for Interpretive Near-Infrared Spectroscopy, 2nd edition, CRC Press, 2012, https://doi.org/10.1201/b11894.